Symbolic-Numeric Solving Boundary Value Problems: Collective Models of Atomic Nuclei

Balt Batgerel[1], Ochbadrakh Chuluunbaatar[1,2,3], Vladimir L. Derbov[4], Alexander A. Gusev[2,5(✉)], Luong Le Hai[6], Algirdas Deveikis[7], Peter O. Hess[8,9], Evgenii V. Mardyban[2], Mariia A. Mardyban[2,5], Sergue I. Vinitsky[2,10], and Peiwei Wen[11]

[1] Institute of Mathematics and Digital Technology, Mongolian Academy of Sciences, Ulaanbaatar, Mongolia
[2] Joint Institute for Nuclear Research, Dubna, Russia
[3] Department of Mathematics, School of Applied Sciences, Mongolian University of Science and Technology, Ulaanbaatar, Mongolia
[4] N.G. Chernyshevsky Saratov National Research State Uiversity, Saratov, Russia
[5] Dubna State University, Dubna, Russia
gooseff@jinr.ru
[6] Ho Chi Minh City University of Education, Ho Chi Minh City, Vietnam
[7] Department of Applied Informatics, Vytautas Magnus University, Kaunas, Lithuania
[8] Instituto de Ciencias Nucleares, UNAM, Circuito Exterior, Mexico D.F., Mexico
[9] Frankfurt Institute for Advanced Studies, 60438 Frankfurt am Main, Germany
[10] Peoples' Friendship University of Russia (RUDN University), Moscow, Russia
[11] China Institute of Atomic Energy, Beijing 102413, China

Abstract. Computational schemes of the Galerkin type method (GTM) and finite elements method (FEM) for solving elliptic multidimensional boundary value problems (BVPs) with variable coefficients of derivatives in a polyhedral d-dimensional domain, aimed at describing collective models of atomic nuclei are presented.

The solution is sought in the form of an expansion in the GTM basis and/or in the FEM basis of piecewise polynomial functions constructed in analytical form by joining Hermite interpolation polynomials and their derivatives at the boundaries of neighboring finite elements, which have the form of d-dimensional parallelepipeds.

The BVPs are formulated and analyzed for collective models including the mixed derivative of the two-dimensional vibrational part of the five-dimensional Hamiltonian in the representation of the nuclear spin angular momentum in the intrinsic reference frame defined by three Euler angles. Benchmark calculations demonstrate performance and robustness of the approach when applied to calculate the lower part of the energy spectrum and the reduced electric transition probabilities in quadrupole collective models of atomic nuclei.

The calculations of the band spectrum of ^{154}Gd isotope using tabulated variable coefficients of the BVP evaluated in the self-consistent relativistic mean-field model revealed a possibility of quasicrossing of

energy levels belonging to different rotational bands of a nucleus at high spin values.

1   Introduction

The finite elements method (FEM) is widely applied to solve elliptic boundary value problems (BVPs). In this method, the domain of independent variables is divided into finite elements. The solution is sought in the form of an expansion in the basis of piecewise polynomial functions constructed in analytical form by joining interpolation polynomials at the boundaries of adjacent finite elements. This leads to a generalized algebraic problem with sparse matrices and saves computer resources [1]. However, to solve the BVPs of collective atomic nuclear models, Galerkin type methods (GTMs) (or Generalized Trefftz Method) are conventionally applied, which use an appropriate basis defined throughout the domain of independent variables. The method reduces the BVP to an algebraic problem with non-sparse matrices, acceptable, e.g., in the quadrupole case [2–11], but rather cumbersome in the quadrupole-octupole case [12] or the multipole case [13].

Alternative FEM calculation schemes for solving the BVPs of collective nuclear models were proposed and applied back in [14–16], but had no wide implementation. FEM schemes have been developed in [17–19] that provide an independent ground to solve the arising multidimensional problems [20]. In recent paper [19], new calculation schemes and symbolic-numeric high-order FEM algorithms for solving multidimensional BVPs [20] were tested in benchmark calculations of the quadrupole spectrum E_{In}, quadrupole moments $Q(I, n)$, and the reduced probabilities of electric interband and intraband $B(E2)$ transitions in ^{190}Os atomic nucleus and other isotopes of several nuclei. It was done in the framework of the geometric quadrupole collective model (GCM) [10] without mixed derivatives in the two-dimensional vibrational part of the five-dimensional Hamiltonian in the representation of $SO(3)$ group of angular momentum I in the intrinsic frame. For this purpose, the 2DFEM program [18] was used implemented for analytical form of BVP variable coefficients in computer algebra systems (CASs) [19]. The results were in good agreement with the calculations of Ref. [8], which used the algebraic version of GTM with five-dimensional harmonic oscillator (5DHO) basis [4].

In the present paper, we report the extended GTM and FEM formulation of a multidimensional BVP for collective models of atomic nuclei with mixed derivatives in the vibrational part of the five-dimensional Hamiltonian in the angular momentum representation in the intrinsic frame [15,16]. We perform and analyse benchmark calculations of the lower part of the energy spectrum for the BVPs for the model, exactly solvable in affine coordinates and the quadrupole collective

model with tabulated variable coefficients given by the self-consistent relativistic mean-field (RMF) model [7]. The calculations of the quadrupole spectrum E_{In} of the ^{154}Gd isotope and of the corresponding reduced electric interband and intraband $B(E2)$ transitions for the RMF-based model revealed a possibility of quasi-crossing of energy levels belonging to rotational bands of a nucleus at high spin values. For this purpose, an adapted version of the algorithm and 2DFEM program from [19] implemented in CAS Mathematica [21] was used.

The paper is organised as follows. Section 2 formulates the d-dimensional BVP and the scheme to solve it using GTM and FEM with Hermite interpolation polynomials (HIPs) on rectangles. Section 3 presents the BVP formulation of the atomic nucleus collective model with mixed derivatives in the vibrational part of the five-dimensional Hamiltonian in the angular momentum representation in the intrinsic reference frame. Sections 4 and 5 are devoted to the analysis of benchmark calculations of the lower part of quadrupole spectrum of a BVP with variable coefficients known in the analytical or tabular form. In Conclusion, the results are discussed and the prospects are outlined.

All calculations were performed using Mathematica 12 on a PC with Intel Core CPU 3.60 GHz, memory 32 Gb, Windows 10 Pro.

2   Formulation of BVP and GTM and FEM Schemes

Consider a self-adjoint BVP for the elliptic differential equation

$$(T + V(x) - E)\,\Phi(x) = 0, \quad T = -\frac{1}{g_0(x)} \sum_{i,j=1}^{d} \frac{\partial}{\partial x_i} g_{ij}(x) \frac{\partial}{\partial x_j}. \tag{1}$$

For the principal part of Eq. (1), the condition of uniform ellipticity holds in the bounded domain $x = (x_1, \ldots, x_d) \in \Omega$ of the Euclidean space $\mathcal{R}^d$, i.e., the constants $\mu > 0$, $\nu > 0$ exist such that

$$\mu \xi^2 \le \sum_{ij=1}^{d} g_{ij}(x) \xi_i \xi_j \le \nu \xi^2, \quad \xi^2 = \sum_{i=1}^{d} \xi_i^2, \quad \forall \xi_i \in \mathcal{R}. \tag{2}$$

The left-hand side of this inequality expresses the requirement of ellipticity, while the right-hand side expresses the boundedness of the coefficients $g_{ij}(x)$. It is assumed that $g_0(x) > 0$, $g_{ji}(x) = g_{ij}(x)$ and $V(x)$ are real-valued functions, continuous with their generalized derivatives up to a given order in a bounded polyhedral domain $x = (x_1, \ldots, x_d) \in \bar{\Omega} = \Omega \cup \partial\Omega \in \mathcal{R}^d$, with the boundary $S = \partial\Omega$, which ensures the existence of nontrivial solutions $\Phi(x)$, corresponding to real-valued eigenvalues E and satisfying the Dirichlet of Neumann boundary conditions [20].

The expansion of the sought solution $\Phi_m^h(x)$ from the Sobolev space $\mathcal{H}_2^{\kappa^c + 1 \ge 1}$ $(\bar{\Omega})$ in the appropriate basis of functions $N_l(x)$ on the domain $\bar{\Omega}$ in the Galerkin type method, see, e.g., [3,4,9,10], has the form

$$\Phi_m^h(x) = \sum_{l=1}^{L_\Omega} N_l(x) \Phi_{lm}^h. \tag{3}$$

In FEM, the polyhedral domain $\bar{\Omega}$: $\bar{\Omega} = \bar{\Omega}_h(x) = \bigcup_{q=1}^{Q} \Delta_q, \quad \bar{\Omega} \subset \mathcal{R}^d$ is divided into subdomains Δ_q, called finite elements. In each of them, local basis functions $\hat{\varphi}_{rq}^{\kappa p'}(x)$, $x \in \mathcal{R}^d$, Lagrange interpolation polynomials (LIPs) or Hermite interpolation polynomials (HIPs) of the order p', are introduced. Here we use the multi-index notation: κ determines the derivative order and direction, r is the local number of a node.

In this case, in expansion (3) we use the piecewise polynomial functions (PPFs) $N_l(x) \equiv N_l^{p'}(x) \in C^{\kappa^c}$ of the order p' with continuous derivatives to a given order constructed by joining the polynomials $\hat{\varphi}_{rq}^{\kappa p'}(x)$ on the finite elements $\Delta_q \in \bar{\Omega}_h(x)$

$$N_l^{p'}(x) \equiv N_s^{\kappa p'}(x) = \bigcup_{q=1}^{Q} \{\hat{\varphi}_{rq}^{\kappa p'}(x) | x \in \Delta_q\}. \tag{4}$$

Here l is determined in terms of multi-indices $\kappa = \kappa_1, \ldots, \kappa_d$ and $r = r_1, \ldots, r_d$; the node number $s = (s_1, \ldots, s_d)$ is related to the local number r of the same node and the finite element number q. Usually, in FEM with HIPs, the piecewise polynomial functions (PPFs) $N_s^{\kappa p'}(x_{s'})$ satisfy the conditions [20]

$$N_s^{\kappa p'}(x_{s'}) = \delta_{ss'}\delta_{\kappa 0}, \quad \left.\frac{\partial^{|\kappa'|}}{\partial x^{\kappa'}} N_s^{\kappa p'}(x)\right|_{x=x_{s'}} = \delta_{ss'}\delta_{\kappa\kappa'}, \quad \frac{\partial^{|\kappa'|}}{\partial x^{\kappa'}} = \frac{\partial^{\kappa_1'}}{\partial x_1^{\kappa_1'}} \cdots \frac{\partial^{\kappa_d'}}{\partial x_d^{\kappa_d'}}.$$

A detailed description of the algorithm for generating multivariate HIPs $\hat{\varphi}_{rq}^{\kappa p'}(x)$ on parallepipeds is given in [18,19]. The HIPs $\hat{\varphi}_{rq}^{\kappa p'}(x)$ of d variables are calculated in the analytical form as a product of HIPs in each variable $\varphi_{r_s q}^{\kappa_s p'}(\bar{x}_s)$ of the order p',

$$\hat{\varphi}_{rq}^{\kappa p'}(x) = \prod_{s=1}^{d} \varphi_{r_s q}^{\kappa_s p'}(\bar{x}_s). \tag{5}$$

$\varphi_{r_s q}^{\kappa_s p'}(\bar{x}_s)$ are calculated in advance analytically by means of recurrence relations implemented in CAS [20,22].

Using expansion (3) with the basis functions $N_l(x)$ of the GPT, or the PPFs $N_l^{p'}$ (4) of FEM, we reduce the BVP (1) to the algebraic generalized eigenvalue problem

$$(\mathbf{A} - \mathbf{B}E_m^h)\mathbf{\Phi}_m^h = 0, \quad (\mathbf{\Phi}_m^h)^T \mathbf{B}\mathbf{\Phi}_m^h = 1, \tag{6}$$

with respect to unknowns E_m^h and $\mathbf{\Phi}_m^h$. The elements of symmetric matrices of stiffness $\mathbf{A} = (A_{ll'})$ and mass $\mathbf{B} = (B_{ll'})$ with the dimension $L_\Omega \times L_\Omega$ are given in [19], and they are calculated on the domain $\bar{\Omega}$ in the Galerkin type method, or on a set Q of the finite elements $\Delta_q \in \bar{\Omega}_h(x)$ in the FEM, by using the appropriate Gaussian quadratures.

Problem (6) is solved by standard numerical methods, implemented as either built-in procedures, e.g., Eigensystem[] procedure in Mathematica [21].

The estimates of the approximate solution E_m^h, $\Phi_m^h(x) \in \mathcal{H}_2^{\kappa^c+1\geq 1}(\Omega_h)$ with respect to the exact solution E_m, $\Phi_m(x) \in \mathcal{H}_2^2(\Omega)$, are as follows [1]:

$$\left| E_m - E_m^h \right| \leq c_1 h^{2p'}, \quad \left\| \Phi_m(x) - \Phi_m^h(x) \right\|_0 \leq c_2 h^{p'+1}, \tag{7}$$

where h is the maximum size of a finite element Δ_q, p' is the FEM scheme order, $c_1 > 0$ and $c_2 > 0$ are the coefficients independent of h, and $h \sim L_\Omega^{-p}$ can be used for GTM [23],

$$\|\Phi_m(x)\|_0^2 = \int_\Omega g_0(x)\, \Phi_m(x) \Phi_m(x)\, dx. \tag{8}$$

3 BVP for Five-Dimensional Quadrupole Hamiltonian

The quadrupole collective model of atomic nuclei is formulated as a BVP for a 5-dimensional anharmonic oscillator with purely discrete spectrum of energy eigenvalues $E_{In} = E_{I1} < E_{I2} < \cdots$ of rotational-vibrational bands of atomic nuclei with spin I in the form of an integer angular momentum. The formalism becomes simpler when the collective variables α_m at $m = -2, -1, 0, 1, 2$ for the 5-dimensional anharmonic oscillator in the laboratory frame are expressed in terms of the collective variables $a_{m'} = a_{m'}(\beta, \gamma)$ in the intrinsic frame of the body-fixed principal axis system by the relations [24]

$$\alpha_m = \sum_{m'} D_{mm'}^{2*}(\theta_i) a_{m'}, \tag{9}$$

$$a_{-2} = a_2 = \frac{\beta \sin(\gamma)}{\sqrt{2}}, \quad a_{-1} = a_1 = 0, \quad a_0 = \beta \cos(\gamma),$$

where $D_{mm'}^{2*}(\theta_i)$ is the Wigner function of irreducible representation of the $O(3)$ group in the intrinsic frame (* denotes complex conjugate).

The five-dimensional quadrupole Hamiltonian in the intrinsic frame parameterized by two internal variables $x_1 = \beta, x_2 = \gamma$ and three Euler angles $x_i = \theta_{i-2}$, $i = 3, 4, 5$, i.e., $x = (x_1, \ldots, x_5) \in \bar{\Omega}_5 = \Omega_5 \cup \partial\Omega_5 \in \mathcal{R}^5$, has the form [15,16]

$$\hat{H} = \frac{\hbar^2}{2}(\hat{T}_{\mathrm{vib}}(x_1, x_2) + \hat{T}_{\mathrm{rot}}(x)) + V(x_1, x_2). \tag{10}$$

Here $\hbar$ is the Planck's constant, $V = V(x_1, x_2)$ is the potential energy, $\hat{T}_{\mathrm{vib}} = \hat{T}_{\mathrm{vib}}(x_1, x_2)$ is the vibrational kinetic energy, and $\hat{T}_{\mathrm{rot}} = \hat{T}_{\mathrm{rot}}(x)$ is the rotational

kinetic energy defined by the relations:

$$\hat{T}_{\text{vib}}(x_1, x_2) = -\frac{1}{g_0(x_1, x_2)} \sum_{i,j=1}^{2} \frac{\partial}{\partial x_i} g_{ij}(x_1, x_2) \frac{\partial}{\partial x_j},$$

$$\hat{T}_{\text{rot}}(x) = \frac{\hat{I}_1^2}{J_1} + \frac{\hat{I}_2^2}{J_2} + \frac{\hat{I}_3^2}{J_3},$$

$$g_0(x_1, x_2) = BB_J \beta^4 \sin(3\gamma) = \frac{1}{2} \beta B |J_1 J_2 J_3|^{1/2},$$

$$g_{11}(x_1, x_2) = \frac{B_J}{B} \beta^4 \sin(3\gamma) B_{\gamma\gamma} = \frac{\beta B_{\gamma\gamma} |J_1 J_2 J_3|^{1/2}}{2B}, \tag{11}$$

$$g_{22}(x_1, x_2) = \frac{B_J}{B} \beta^2 \sin(3\gamma) B_{\beta\beta} = \frac{B_{\beta\beta} |J_1 J_2 J_3|^{1/2}}{2\beta B},$$

$$g_{12}(x_1, x_2) = g_{21}(x_1, x_2) = -\frac{B_J}{B} \beta^3 \sin(3\gamma) B_{\beta\gamma} = -\frac{B_{\beta\gamma} |J_1 J_2 J_3|^{1/2}}{2B}.$$

Here $B = \sqrt{B_{\beta\beta} B_{\gamma\gamma} - B_{\beta\gamma}^2}$ is the square root of the determinant of the two-dimensional matrix of vibrational function coefficients (i.e., the vibrational part of the inertia tensor), $B_{\beta\beta} \equiv B_{\beta\beta}(\beta, \gamma)$, $B_{\gamma\gamma} \equiv B_{\gamma\gamma}(\beta, \gamma)$, and $B_{\beta\gamma} \equiv B_{\beta\gamma}(\beta, \gamma)$; $B_J = \sqrt{B_1 B_2 B_3}$ is a square root of the determinant of the three-dimensional diagonal matrix of rotational function coefficients $B_1 \equiv B_1(\beta, \gamma)$, $B_2 \equiv B_2(\beta, \gamma)$, and $B_3 \equiv B_3(\beta, \gamma)$. $\hat{I}_1$, $\hat{I}_2$, and $\hat{I}_3$ are components of the angular momentum $\hat{I}$ in terms of the Euler angles of the intrinsic frame. The moments of inertia $J_k \equiv J_k(\beta, \gamma)$ of the intrinsic frame are denoted as

$$J_k(x_1, x_2) = J_k(\beta, \gamma) = 4B_k(\beta, \gamma) \beta^2 \sin^2(\gamma - 2\pi k/3), \quad k = 1, 2, 3. \tag{12}$$

The Schrödinger equation with respect to eigenfunction

$$\Psi_{nIM} \equiv \Psi_{nIM}(\beta, \gamma, \vartheta_i)$$

and the corresponding eigenvalues of energy E_{In} has the form

$$(\hat{H} - E_{In}) \Psi_{nIM} = 0. \tag{13}$$

The eigenfunction Ψ_{nIM} in the representation of the angular momentum I and its projections K and M on the third axes of the intrinsic and laboratory frames can be written as [24]

$$\Psi_{nIM}(\beta, \gamma, \vartheta_i) = \sum_{K \geq 0,\, \text{even}}^{I} \mathcal{D}_{MK}^{I*}(\vartheta_i) \Phi_{nIK}(\beta, \gamma), \tag{14}$$

where $\mathcal{D}_{MK}^{I*}(\vartheta_i)$ are the normalized D-functions with the space parity $\hat{\pi} = \pm 1$

$$\mathcal{D}_{MK}^{I*}(\vartheta_i) = \sqrt{\frac{2I+1}{8\pi^2}} \frac{(D_{MK}^{I*}(\vartheta_i) + \hat{\pi}(-1)^I D_{M-K}^{I*}(\vartheta_i))}{\sqrt{2(1 + \delta_{K0})}}. \tag{15}$$

The operator of rotational energy $\hat{T}_{\text{rot}}$ reads as [24]

$$\hat{T}_{\text{rot}} = \sum_{i=1}^{3} \frac{\hat{I}_i^2}{J_i} = (\hat{I}^2 - \hat{I}_3^2)\left(\frac{1}{2J_1} + \frac{1}{2J_2}\right) + \frac{\hat{I}_3^2}{J_3} + (\hat{I}_+^2 + \hat{I}_-^2)\left(\frac{1}{4J_1} - \frac{1}{4J_2}\right),$$

where the action of the operators $\hat{I}^2 = \hat{I}_1^2 + \hat{I}_2^2 + \hat{I}_3^2 = (\hat{I}_+\hat{I}_- + \hat{I}_-\hat{I}_+)/2 + \hat{I}_3^2$ and $\hat{I}_\pm = \hat{I}_1 \pm \imath I_2$ is determined by the relations

$$\hat{I}^2 D_{MK}^{I*}(\vartheta_i) = I(I+1)D_{MK}^{I*}(\vartheta_i),$$
$$\hat{I}_3 D_{MK}^{I*}(\vartheta_i) = K D_{MK}^{I*}(\vartheta_i),$$
$$\hat{I}_\pm D_{MK}^{I*}(\vartheta_i) = \sqrt{I(I+1) - K(K \mp 1)} D_{MK-1}^{I*}(\vartheta_i).$$

Functions Ψ_{nIM} obey Neumann or Dirichlet boundary conditions at the boundary $\partial\Omega_5$ of domain Ω_5, as well as orthogonality and normalization conditions

$$\int_{\Omega_5} \Psi_{nIM}^* \Psi_{n'I'M'} g_0(\beta,\gamma) d\beta d\gamma \sin(\vartheta_2) d\vartheta_1 d\vartheta_2 d\vartheta_3 = \delta_{nn'}\delta_{II'}\delta_{MM'}. \quad (16)$$

The unknown set of $I_{\max}$ internal components $\Phi_{nIK} \equiv \Phi_{nIK}(\beta,\gamma)$, where $K = 0, 2, \ldots, I$ for even I, or $K = 2, 4, \ldots, (I-1)$ for odd I, compose the vector eigenfunction Φ_{nI} corresponding to the eigenvalue E_{In} (in MeV) of the BVP for a system of $I/2 + 1$ or $(I-1)/2$ equations for even or odd I, respectively:

$$\left[\hat{T}_{\text{vib}} + T_{KK}^I + \frac{2}{\hbar^2}(V - E_{In})\right]\Phi_{nIK} + T_{KK+2}^I \Phi_{nIK+2} + T_{KK-2}^I \Phi_{nIK-2} = 0,$$

$$T_{KK}^I = (I(I+1) - K^2)\left(\frac{1}{2J_1} + \frac{1}{2J_2}\right) + \frac{K^2}{J_3}, \quad (17)$$

$$T_{KK\pm2}^I = \left(\frac{1}{4J_1} - \frac{1}{4J_2}\right)C_{KK\pm2}^I,$$

$$C_{KK-2}^I = (1+\delta_{K2})^{1/2}[(I+K)(I-K+1)(I+K-1)(I-K+2)]^{1/2}, \quad (18)$$

$$C_{KK+2}^I = (1+\delta_{K0})^{1/2}[(I-K)(I+K+1)(I-K-1)(I+K+2)]^{1/2},$$

where $\hat{T}_{\text{vib}}$ and J_1, J_2, J_3 are given in (11) and (12). The components Φ_{nIK} are subject to Neumann or Dirichlet boundary conditions at the boundary $\partial\Omega_2$ of the domain Ω_2 [15,16], and the orthogonality and normalization conditions

$$\int_0^{\beta_{\max}} \int_0^{\pi/3} g_0(\beta,\gamma) d\beta d\gamma \sum_{K\geq0,even}^{I_{\max}} \Phi_{nIK}(\beta,\gamma)\Phi_{n'IK}(\beta,\gamma) = \delta_{nn'}. \quad (19)$$

4   5D Harmonic Oscillator Model in Affine Coordinates

To show the applicability of FEM schemes and the adapted 2DFEM program implemented in Mathematica we present benchmark calculations of exact solvable model of the 5DHO with parameters $B_{\beta\beta} = B_{\gamma\gamma} = B_0$, $B_{\beta\gamma} = B_{\gamma\beta} = 0$, $B_1 = B_2 = B_3 = B_0$, and J_1, J_2, J_3 from (12), and potential $V(\beta,\gamma) = (C_2/2)\beta^2$,

Table 1. The discrepancies $\delta E_{I,n=1} = E_{I,n=1}^{\text{num}} - E_{I,n=1}$ of the eigenvalues $E_{In=1}$ of the 5DHO model in coordinates (β, γ) (left panel) and (b_0, b_2) (right panel) and Runge coefficients (20) (Ru) by the FEM schemes with HIPs of the order $p' = 2, 3, 4, 5$, and the multiplicity κ'.

(p',κ')	I	h	$h/2$	$h/4$	Ru
(2,0)	0	9.6(-5)	6.1(- 6)	3.8(- 7)	3.98
	2	1.2(-4)	7.9(- 6)	5.3(- 7)	3.97
	3	1.4(-4)	1.5(- 5)	6.8(- 6)	3.97
(3,0)	0	5.4(-6)	9.2(- 8)	1.5(- 9)	5.88
	2	9.6(-6)	1.6(- 7)	2.6(- 9)	5.92
	3	1.4(-5)	4.2(- 7)	1.9(- 7)	5.93
(3,1)	0	1.4(-5)	2.8(- 7)	4.7(- 9)	5.62
	2	2.2(-5)	4.7(- 7)	8.3(- 9)	5.57
	3	2.9(-5)	1.2(- 6)	5.9(- 7)	5.47
(4,0)	0	8.5(-7)	3.3(- 9)	1.3(-11)	8.01
	2	1.2(-6)	7.1(- 9)	2.9(-11)	7.43
	3	3.7(-6)	1.6(- 8)	2.1(- 9)	8.11
(4,1)	0	1.4(-6)	3.8(- 9)	1.4(-11)	8.47
	2	2.1(-6)	8.6(- 9)	3.0(-11)	7.95
	3	7.5(-6)	1.9(- 8)	2.5(- 9)	8.78
(5,0)	0	4.1(-9)	8.7(-12)	1.2(-14)	8.89
	2	1.9(-8)	2.2(-11)	-3.0(-13)	9.75
	3	4.4(-8)	6.0(-11)	6.2(-12)	9.68
(5,1)	0	8.6(-9)	1.5(-11)	-5.3(-15)	9.11
	2	2.5(-8)	3.8(-11)	1.8(-13)	9.34
	3	5.5(-8)	1.0(-10)	1.3(-11)	9.24
(5,2)	0	3.4(-8)	2.5(-11)	-1.1(-13)	10.38
	2	8.6(-8)	6.8(-11)	7.5(-14)	10.30
	3	2.1(-7)	2.1(-10)	1.9(-11)	10.15

(p',κ')	I	h	$h/2$	$h/4$	Ru
(2,0)	0	2.8(-3)	2.2(-4)	1.4(- 5)	3.68
	2	5.6(-3)	4.0(-4)	2.6(- 5)	3.80
	3	1.2(-2)	8.4(-4)	5.5(- 5)	3.87
(3,0)	0	3.1(-4)	8.0(-6)	1.3(- 7)	5.28
	2	9.2(-4)	1.5(-5)	2.6(- 7)	5.92
	3	2.8(-3)	4.4(-5)	7.6(- 7)	6.03
(3,1)	0	4.8(-4)	1.8(-5)	3.9(- 7)	4.68
	2	1.2(-3)	3.3(-5)	7.4(- 7)	5.20
	3	3.3(-3)	8.6(-5)	2.1(- 6)	5.27
(4,0)	0	2.7(-5)	1.4(-7)	6.0(-10)	7.64
	2	8.2(-5)	3.7(-7)	1.6(- 9)	7.80
	3	2.2(-4)	1.3(-6)	5.5(- 9)	7.44
(4,1)	0	4.7(-5)	1.9(-7)	6.8(-10)	7.92
	2	1.5(-4)	5.5(-7)	1.8(- 9)	8.07
	3	3.9(-4)	2.0(-6)	6.4(- 9)	7.58
(5,0)	0	4.3(-6)	5.2(-9)	7.0(-12)	9.66
	2	9.9(-6)	1.6(-8)	1.7(-11)	9.28
	3	3.2(-5)	6.2(-8)	7.1(-11)	9.01
(5,1)	0	4.6(-6)	6.9(-9)	1.1(-11)	9.37
	2	1.1(-5)	2.0(-8)	3.0(-11)	9.09
	3	3.7(-5)	7.5(-8)	1.2(-10)	8.95
(5,2)	0	2.0(-5)	2.6(-8)	1.8(-11)	9.62
	2	4.0(-5)	8.1(-8)	5.1(-11)	8.96
	3	9.7(-5)	3.1(-7)	2.2(-10)	8.29

$$g_0(\beta,\gamma) = B_0^{5/2}\beta^4 \sin(3\gamma), \quad g_{11}(\beta,\gamma) = \frac{g_0(\beta,\gamma)}{B_0},$$

$$g_{22}(\beta,\gamma) = \frac{g_0(\beta,\gamma)}{B_0\beta^2}, \quad g_{12}(\beta,\gamma) = g_{21}(\beta,\gamma) = 0.$$

In this case, the operator T_{vib} has no mixed partial derivatives and the spectrum and eigenfunctions is known in an analytical form [10] as well as in internal coordinates (a_0, a_2):

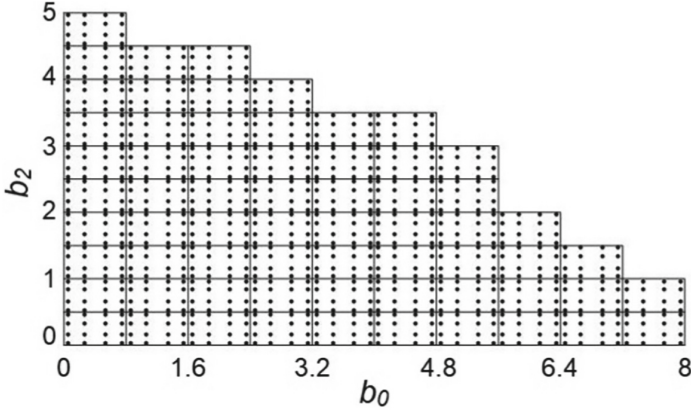$$a_0 = \beta \cos(\gamma), \quad a_2 = \frac{1}{\sqrt{2}}\beta \sin(\gamma),$$

$$g_0(a_0, a_2) = 2B_0^{5/2}(3a_0^2 - 2a_2^2)a_2, \quad g_{11}(a_0, a_2) = \frac{g_0(a_0, a_2)}{B_0},$$

$$g_{22}(a_0, a_2) = \frac{g_0(a_0, a_2)}{2B_0}, \quad g_{12}(a_0, a_2) = g_{21}(a_0, a_2) = 0,$$

$$V(a_0, a_2) = \frac{C_2}{2}(2a_2^2 + a_0^2),$$

$$J_1 = B_0\frac{(\sqrt{6}a_2 + 3a_0)^2}{3}, \quad J_2 = B_0\frac{(\sqrt{6}a_2 - 3a_0)^2}{3}, \quad J_3 = 8B_0a_2^2.$$

Fig. 1. Nonrectangular region with grid of finite elements for the harmonic oscillator. The Gaussian nodes are marked by circles

The operator T_{vib} has mixed partial derivatives in affine coordinates (b_0, b_2):

$$a_0 = b_0 + \sqrt{\frac{2}{3}}b_2, \quad a_2 = b_2,$$

$$g_0(b_0, b_2) = 2B_0^{5/2}b_0b_2(3b_0 + 2\sqrt{6}b_2), \quad g_{11}(b_0, b_2) = \frac{4g_0(b_0, b_2)}{3B_0},$$

$$g_{22}(b_0, b_2) = \frac{g_0(b_0, b_2)}{2B_0}, \quad g_{12}(b_0, b_2) = g_{21}(b_0, b_2) = -\frac{g_0(b_0, b_2)}{\sqrt{6}B_0},$$

$$V(b_0, b_2) = \frac{C_2}{6}(8b_2^2 + 3b_0^2 + 2\sqrt{6}b_0b_2),$$

$$J_1 = B_0\frac{(2\sqrt{6}b_2 + 3b_0)^2}{3}, \quad J_2 = 3B_0b_0^2, \quad J_3 = 8B_0b_2^2.$$

The discrepancies $\delta E_{I,n=1} = E_{I,n=1}^{\text{num}} - E_{I,n=1}$ of the eigenvalues $E_{In=1}$ of the 5DHO model in coordinates (β, γ) (left panel) and (b_0, b_2) (right panel) are presented in Table 1. The calculations are performed at $B_0 = 1$, $C_2 = 1$, and $\hbar = 1$ on the grids $\Omega_{\beta,\gamma} = [0(h_\beta)7] \otimes [0(h_\gamma)\pi/3]$ with $h_\beta = h, h/2, h/4$ at $h = 7/N_g$ and $h_\gamma = \pi/(3N_g)$ and $\Omega_{b_0,b_2} = ([0(h_0)8] \otimes [0(h_2)5])$ with $h_0 = h, h/2, h/4$, $h_2 = 5h_0/8$ at $h = 8/N_0$. Here $N_g = 20$, 12, 8, and 8 and $N_0 = 10$, 7, 6, and 5 for the $p' = 2$, 3, 4, and 5, respectively. In grid Ω_{b_0,b_2}, the cells Δ_q for which $\min_{(b_0,b_2)\in\Delta_q} V(b_0, b_2) > 30$ are dropped (see, for example, Fig. 1).

The Runge coefficients were calculated in the grids $\Omega_{\beta,\gamma}$ and Ω_{b_0,b_2}

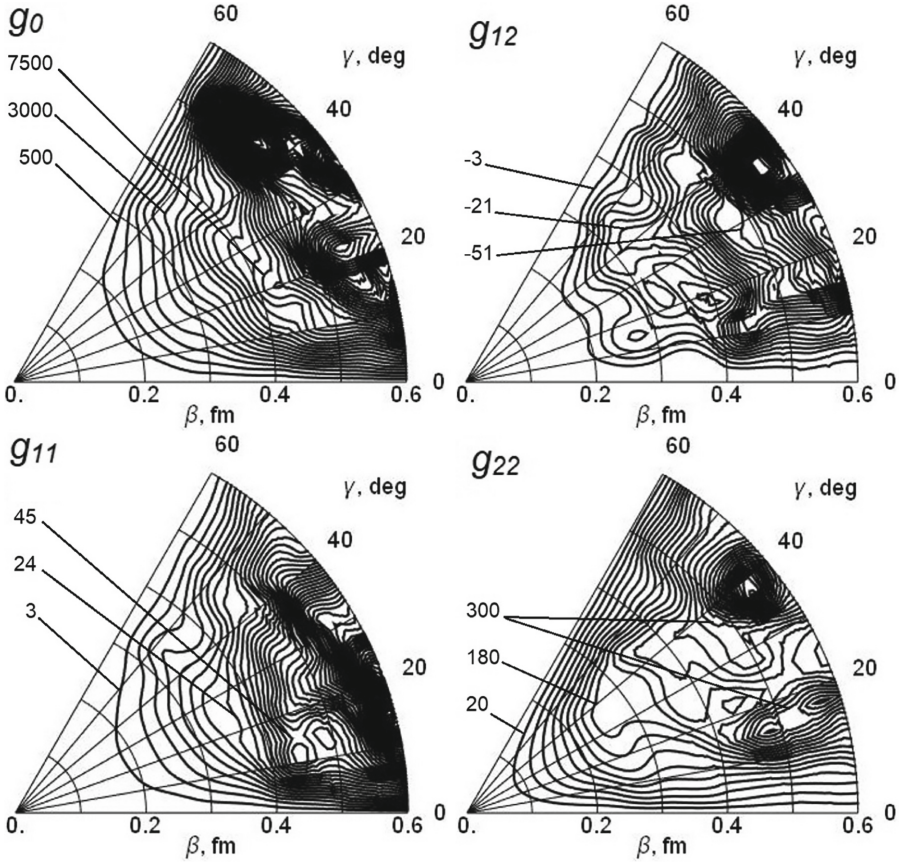$$r_h = \log_2 \left| \frac{(E_{In})_h - (E_{In})_{h/2}}{(E_{In})_{h/2} - (E_{In})_{h/4}} \right|, \tag{20}$$

Fig. 2. Isolines of $g_0(\beta, \gamma)$ and $g_{ij}(\beta, \gamma)$ of ^{154}Gd

where $(E_{In})_h$, $(E_{In})_{h/2}$, and $(E_{In})_{h/4}$ are the energies calculated by the program 2DFEM on the doubly condensed grids, gave estimates presented in Table 1 confirming the theoretical estimate (7) of the order of $2p' \approx 4, 6, 8, 10$.

5   Benchmark Calculations of ^{154}Gd in the RMF Model

In this case, the metric tensor coefficients g_{11}, $g_{12} = g_{21}$, g_{22} and g_0, and the potential energy V, (see, e.g., Figs. 2 and 3), were calculated using an appropriate approximation of the input data, namely, the coefficients of the vibrational part of the inertia tensor $B_{\gamma\gamma}$, $B_{\beta\gamma}$, $B_{\beta\beta}$, the moments of inertia J_1, J_2, J_3, and the potential energy V on the grid $\Omega_{\beta,\gamma}$. The data were calculated within the framework of the RMF model [7,26,27] using the PC-F1 parameterization, where
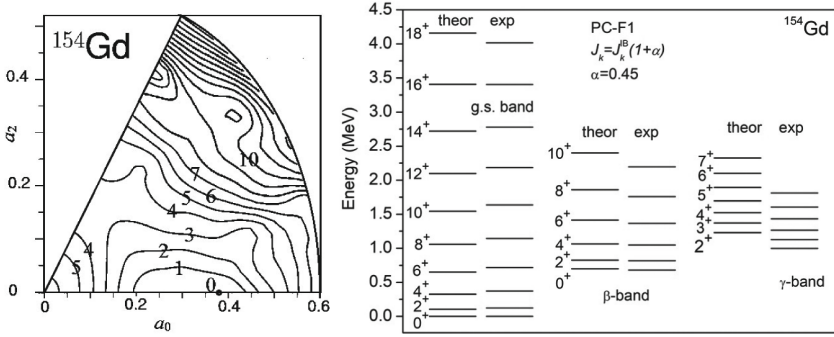
Fig. 3. Isolines of $V(\beta, \gamma)$ for ^{154}Gd counted from the minimum of $V(\beta = 0.3875, \gamma = 0)$ $= -1270.6$ MeV (left); the lower part of the calculated spectrum bands [7], labeled with nuclear spin I and spatial parity $\hat{\pi} = +$, and the experimental data [25] (right)

at $\hbar = 1$ the quantities B, B_J and B_k are related to w, r, and B_k from [7] as

$$w = B^2 = B_{\beta\beta}B_{\gamma\gamma} - B_{\beta\gamma}^2, \quad r = B_J^2 = B_1 B_2 B_3 = \frac{J_1 J_2 J_3}{4\beta^6 \sin^2(3\gamma)},$$

$$B_k = \frac{J_k(\beta, \gamma)}{4\beta^2 \sin^2(\gamma - 2\pi k/3)}, \quad k = 1, 2, 3.$$

Note that when using the PC-F1 parameterization in the calculations of ^{154}Gd, the values J_1 J_2 J_3 were multiplied by the linear scale factor 1.45, i.e., $J_k(q) = (1 + \alpha)J_k^{\text{IB}}(q)$ with $\alpha = 0.45$, as was accepted in [7] and explained in [5, 28, 29].

Table 2 presents the lower part of the ^{154}Gd quadrupole spectrum E_{In} in MeV, (see, e.g., Fig. 3), calculated on the grid $\Omega_{\beta,\gamma}$ using:

– the Galerkin type method with the set of $L_\Omega \approx 50$ basis functions of 5DHO [9] and the interpolation of the input data with steps $h_\beta = 0.025$, $h_\gamma = 10$ degrees by linear S1B and cubic S3B splines in the Gaussian nodes;
– the FEM and S1F, S3F, the same but using a twice condensed FEM grid in the Gaussian nodes of 2DFEM with the HIPs of the third order.

The FEM calculations were carried out on the grid chosen above with an absolute accuracy of the eigenenergy E_{In} not worse than 0.02 MeV. An agreement of FEM and GTM calculations up to three or two significant digits is seen due to using a twice condensed FEM grid, and selective agreement with experimental data due to using the linear scaling factor α instead of unknown nonlinear one [11] and other restrictions inherent in the RMF model parametrization [7].

Figure 4 shows the lower part of the ^{154}Gd spectrum in the diagonal and nondiagonal approximation in comparison with experimental results for each of A, B, E, C, G, and I bands used in the experimental data tables [25]:

Table 2. The spectrum E_{In} (in MeV) of ^{154}Gd counted from minimum of the potential energy V and from the ground state energy $E_{0,n=1}$ calculated on the grids $\Omega_{\beta,\gamma}$ using the linear (S1) and cubic (S3) spline interpolations of the BVP coefficients: (S1B) and (S3B)—GTM with the basis functions (3) on the grid $\Omega = \{0(0.025)0.6\}\otimes\{0(\pi/18)\pi/3\}$; (S1F) and (S3F)—FEM with (4) and HIPs of the 3rd order on a finite-element grid $\Omega = \{0(0.06)0.6\}\otimes\{0(\pi/30)\pi/3\}$; Exp – the experimental data from [25]

I	n	E_{In}				$E_{In} - E_{0,n=1}$				
		S1B	S3B	S1F	S3F	S1B	S3B	S1F	S3F	Exp [25]
0	1	1.98	2.02	1.90	1.92	0.00	0.00	0.00	0.00	0.00
0	2	2.62	2.63	2.54	2.53	0.64	0.62	0.64	0.62	0.6806673 (18)
0	3	3.51	3.51	3.42	3.41	1.53	1.49	1.53	1.49	1.182091 (4)
2	1	2.07	2.11	1.99	2.01	0.09	0.09	0.09	0.09	0.1230709 (9)
2	2	2.73	2.74	2.65	2.64	0.75	0.72	0.75	0.73	0.8154917 (15)
2	3	3.37	3.40	3.03	3.13	1.39	1.38	1.13	1.21	0.9962568 (16)
3	1	3.50	3.55	3.13	3.23	1.53	1.53	1.23	1.31	1.1278018 (2)
4	1	2.27	2.31	2.19	2.21	0.29	0.29	0.29	0.29	0.3709998 (11)
4	2	2.95	2.96	2.87	2.87	0.97	0.95	0.98	0.95	1.047592 (3)
4	3	3.65	3.69	3.25	3.35	1.67	1.67	1.35	1.43	1.263778 (4)
5	1	3.83	3.87	3.38	3.49	1.85	1.85	1.49	1.57	1.432588 (6)
6	1	2.57	2.61	2.48	2.50	0.59	0.59	0.59	0.59	0.717662 (4)
6	2	3.29	3.30	3.21	3.20	1.31	1.28	1.31	1.29	1.365878 (8)
6	3	4.03	4.06	3.54	3.64	2.05	2.04	1.65	1.73	1.60655 (8)
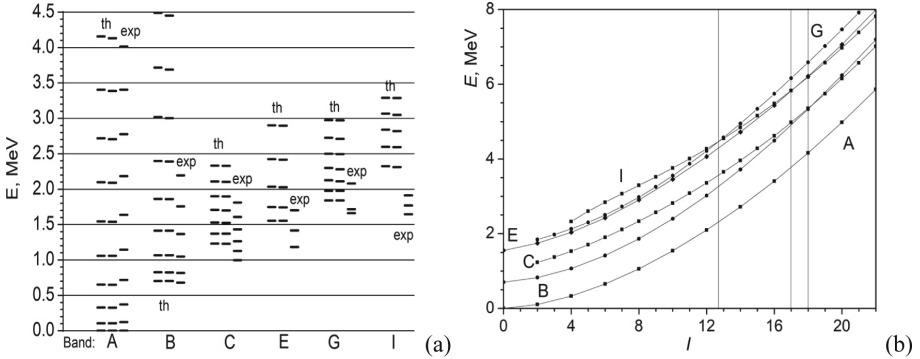
Fig. 4. (a) Energy spectrum of ^{154}Gd. For each state of the bands A, B, E, C, G, and I, three short bars correspond to the diagonal approximation (left), nondiagonal one (middle), and experiment [25] (right). (b) Calculated spectrum of ^{154}Gd plotted vs spin I in the diagonal approximation. The crossing points are marked by vertical lines

Table 3. Correspondence between the notation A, B, E, C, G, I of bands in diagonal approximation of the rotational coupling, the values of nuclear spin I and its leading projection K on the third axis in the intrinsic frame, and the number n of calculated states

| band	K	I	0	2	3	4	5	6	7	8	9	10	11	12	13	14	15	16	17	18	19	20	21	22
A	0	n	1	1		1		1		1		1		1		1		1		1		1		1
B	0	n	2	2		2		2		2		2		2		2		2		**2**		**3**		3
C	2	n		3	1	3	1	3	1	3	1	3	1	3	1	3	1	3	1	**3**	1	**2**	1	2
E	0	n	3	4		4		4		4		4		4		**4**		**5**		5		5		5
G	2	n		5	2	5	2	5	2	5	2	5	2	**5**	**3**	6	3	6	3	6	3	6	3	6
I	4	n				6	3	6	3	6	3	6	3	**6**	**2**	5	2	**5**	2	**4**	2	4	2	4
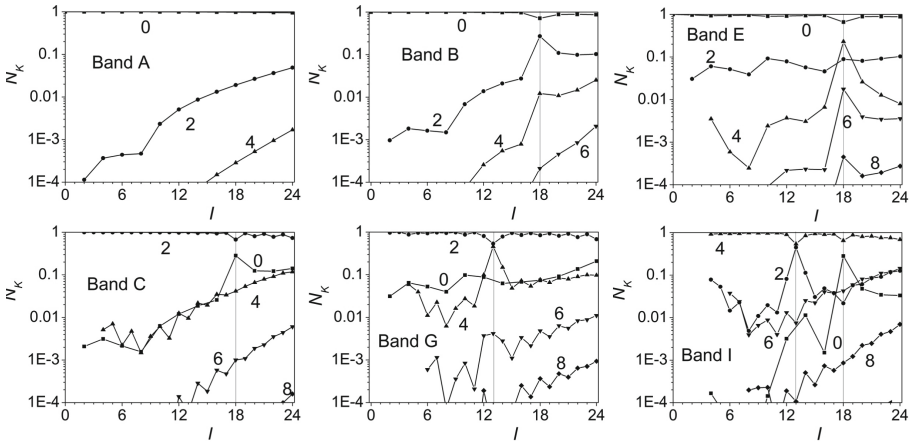
Fig. 5. Integrals $N_K \equiv N^I_{Kn}$ from Eq. (21) for each of A, B, E, C, G, and I bands at the values of $K = 0, 2, 4, 6, 8$ labelling each of the curves

- Band(A) is the $K^\pi = 0+$ ground state band;
- Band(B): the first excited $K^\pi = 0^+$ (β-vibrational) band;
- Band(E), Band(J), Band(K): the second, third and forth excited $K^\pi = 0^+$ bands;
- Band(C): the $K^\pi = 2^+$ (γ-vibrational) band;
- Band(G): the second excited $K^\pi = 2^+$ ($\beta\gamma$-vibrational) band;
- Band(I): the $K^\pi = 4^+$ band.

Table 3 shows the correspondence between the notation A, B, E, C, G, and I of the bands and the values of spin I and its leading projection K on the third axis in the intrinsic frame, and the number n of calculated states. The numbers n of the energy levels belonging to B and C, and E, G, and I bands that have crossing points shown in Fig. 4b are given in boldface.

Table 4. The reduced $B(E2)$ transition probabilities (in W.u.) in (nd) and (diag) – nondiagonal and diagonal approximations, and (exp) – experimental data [25]

| $B(E2)$	nd	diag	exp	bands
$2_1 \to 0_1$	160	159	157	AA
$4_1 \to 2_1$	244	243	245	
$6_1 \to 4_1$	294	293	285	
$8_1 \to 6_1$	341	339	312	
$10_1 \to 8_1$	387	385	360	
$2_2 \to 0_2$	194	193	97.0	BB
$0_2 \to 2_1$	68.5	69.2	52.0	BA
$2_2 \to 4_1$	45.0	45.5	19.6	
$2_3 \to 4_1$	0.460	0.248	1.72	CA
$2_3 \to 0_1$	3.89	4.14	5.70	
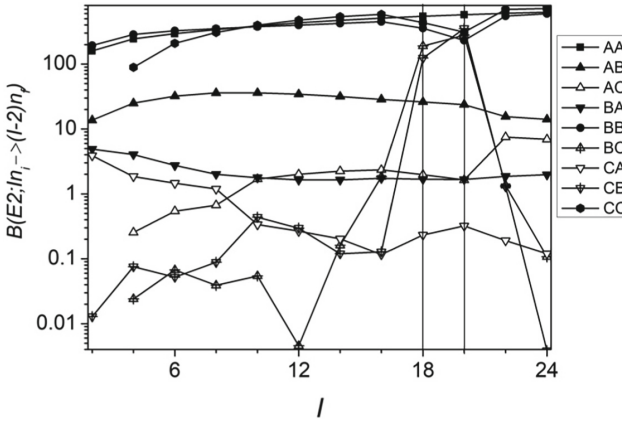
Fig. 6. Calculated intraband and interband $B(E2; In_i \to (I-2)n_f)$ transitions between A, B and C bands in Weisskopf units (W.u.) in the nondiagonal approximation for ^{154}Gd

In Fig. 5 we present the partial probability density integrals of components $\Phi_{nIK}(\beta, \gamma)$ of wave function $\Psi_{nI}(\beta, \gamma, \theta_i)$ for each of A, B, E, C, G, and I bands

$$N_{Kn}^I = \int_0^{\beta_{\max}} \int_0^{\pi/3} g_0(\beta, \gamma) \Phi_{nIK}(\beta, \gamma) \Phi_{nIK}(\beta, \gamma) d\beta d\gamma, \qquad (21)$$

$$\sum_{K \geq 0, \text{even}}^I N_{Kn}^I = 1.$$

The sum of partial integrals satisfies the normalization condition (16) or (19). As can be seen from the Figure, the probability density integrals of the leading
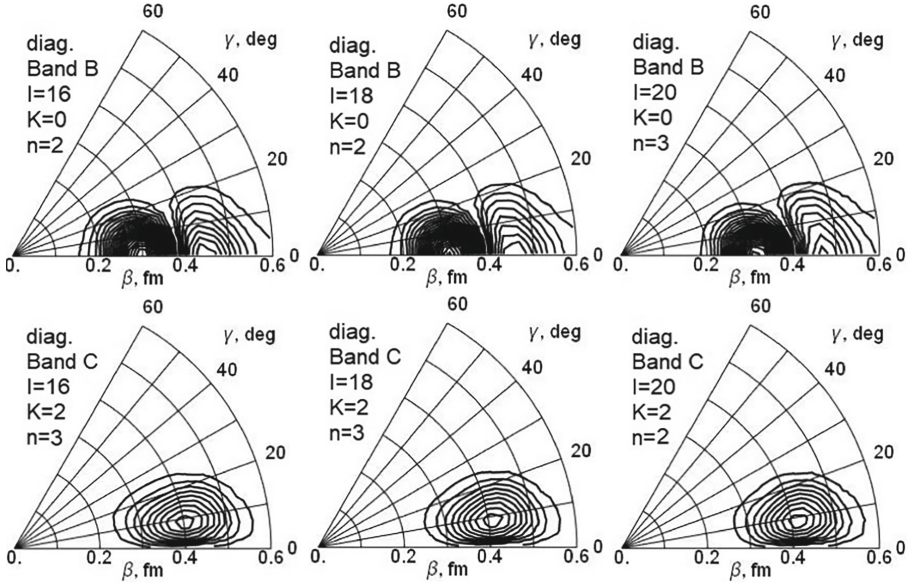
Fig. 7. Isolines of the leading components $\Phi_{nIK} = \pm 0.01, \pm 0.02, \ldots$ of the ^{154}Gd wave functions for $n = 2, 3$ and $I = 16, 18, 20$ in diagonal approximation

component for A, B, and E bands at $K = 0$, for C and G bands at $K = 2$, and for I band at $K = 4$ exceed the other ones by more than 10 times, which confirms the classification of bands accepted for experimental data [25].

From Fig. 4b, an exact crossing of energy levels is seen in the diagonal approximation, for example, of G and I bands, E and I bands, and B and C bands in the vicinity of $I = 13$, $I = 17$, and $I = 18$, respectively. However, when switching on the rotational coupling, i.e., in the nondiagonal approximation, these exact crossings transform into quasi-crossings.

Figure 6 illustrates the calculations of the reduced probabilities of intraband and interband $B(E2; In_i \rightarrow (I-2)n_f)$ transitions [19] between A, B, and C bands in the Weisskopf units (W.u.) in the nondiagonal approximation for ^{154}Gd using the formulas

$$B_{W.u.}(E\lambda) = \frac{e^2}{4\pi}\left(\frac{3}{\lambda+3}\right)^2 R_0^{2\lambda}, \tag{22}$$

where $R_0 = r_0 A^{1/3}$, $r_0 = 1.2$ fm; and $B_{W.u.}(E\lambda) = 0.05940\,A^{4/3}$ in $e^2 fm^4$ units at $\lambda = 2$. In the vicinity of the quasi-crossing point at $I = 18$, the values of interband transitions between B and C bands are approximately 200 W.u., in comparison with small values (< 1 W.u.) beyond the vicinity. However, the intraband transitions in the B and C bands in the vicinity of the quasi-crossing point are approximately by two times smaller than beyond the vicinity. Table 4 presents the intraband and interband $B(E2)$ values calculated in diagonal (diag) and nondiagonal (nd) approximations, in comparison with the known experimental data
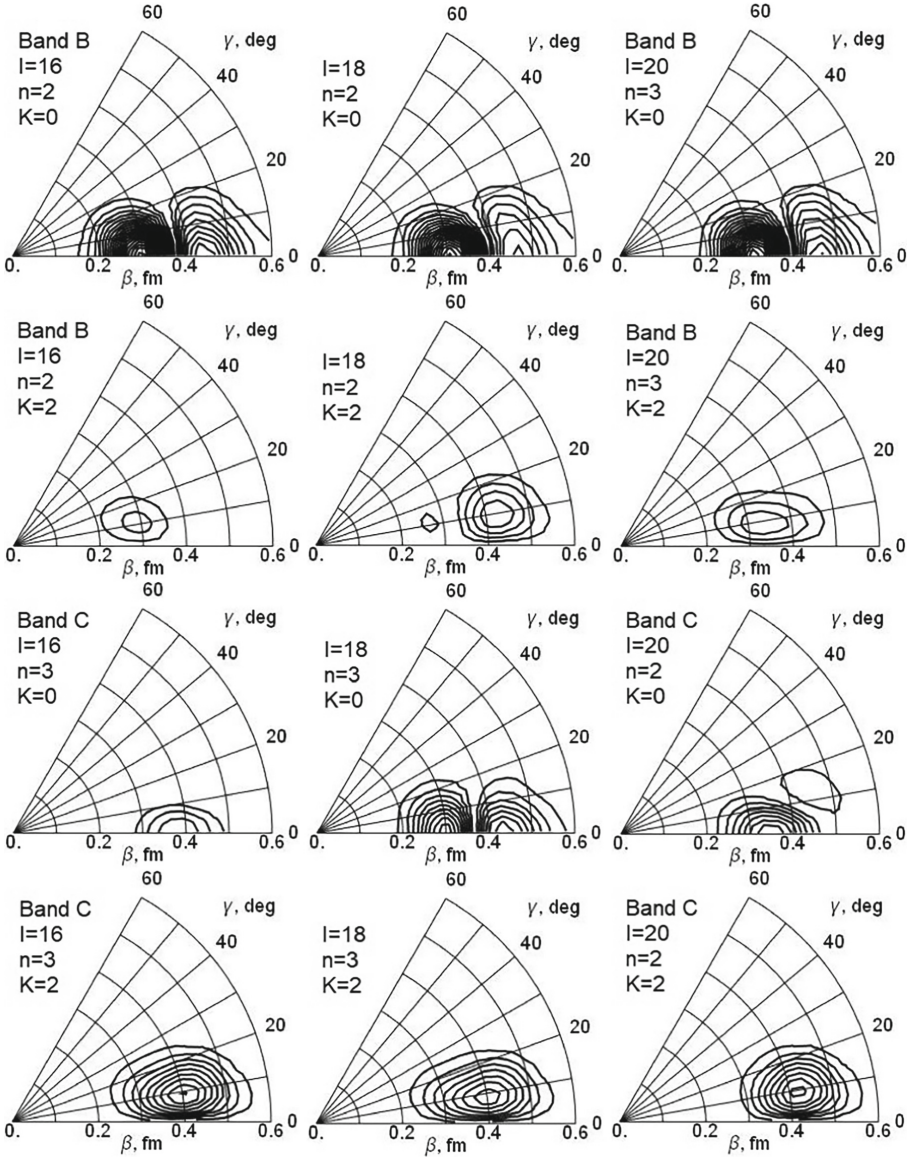
Fig. 8. Isolines of the leading components $\Phi_{nIK} = \pm 0.01, \pm 0.02, \ldots$ of the ^{154}Gd wave functions for $n = 2, 3$ and $I = 16, 18, 20$ in diagonal and nondiagonal approximations

(exp) for ^{154}Gd isotope [25]. The leading values of diagonal approximation do also confirm the experimental classification, while a selected agreement with the experimental data is due to the above restriction of the model parametrization.

Figures 7 and 8 show isolines of the leading components $\Phi_{nIK}(\beta, \gamma)$ for $I = 16, 18,$ and 20: at $n = 2$ and 3 in diagonal and in nondiagonal approximations, respectively, that exceed 0.01 by absolute value at $K = 0$ and $K = 2$.

From Fig. 7, the shape of the components is seen to be practically unchanged at $I = 16$, 18, and 20 in the diagonal approximation. In the nondiagonal approximation (see Fig. 8), at $I = 16$ and $I = 20$, the leading components practically coincide with those in the diagonal approximation, and at $I = 18$, the components are their linear combinations, belonging to both bands.

6   Conclusions

To solve elliptic multidimensional BVPs with variable coefficients of derivatives, high-accuracy FEM schemes have been developed with piecewise polynomial basis functions constructed by joining Hermite interpolation polynomials and their derivatives at the boundaries of neighboring finite elements in the form of parallelepipeds, which will be used in the development of software tools in CAS Mathematica for solving multidimensional BVPs with variable coefficients of partial derivatives specified in both analytical and tabular form [19].

The new version of the algorithm is implemented in the form of the program 2DFEM to solve the BVP arising in the collective models of atomic nuclei with mixed derivatives in the vibrational part of the five-dimensional Hamiltonian. The efficiency of the developed algorithms and programs is demonstrated by benchmark calculations of the lower part of the quadrupole rotational-vibrational spectrum of the 5DHO model in affine coordinates presented in Table 1, which confirm the order $p' = 2, 3, 4, 5$ of the implemented FEM schemes, and the self-consistent RMF model [7] of ^{154}Gd isotope presented in Table 2, which agree with the GTM calculations and demonstrate high performance of the programs even when using a conventional personal computer.

Note that using the nonrectangular region with a finite element mesh on Gaussian nodes tested in Sect. 4 for the harmonic oscillator 1 offers potential saving of computer resources and preserves the accuracy for the case of coefficients of BVP given in tabulated form, whereas the RMF calculations of tabulated coefficients require huge MPI computer resources and the spline interpolation does not ensure required accuracy.

The calculations of the quadrupole spectrum E_{In} of ^{154}Gd isotope and corresponding the reduced probabilities of electric interband and intraband $B(E2)$ transitions for the model based on RMF revealed a possibility of quasi-crossing of energy levels belonging to different bands at some values of the nucleus spin. This allows identifying the existence of such quasi-crossing in the band spectra of other nuclei at high spins [28] in the course of further studies.

The developed approach and programs provide a base for adapting multidimensional FEM programs to solving the bound state problems of the rotational-vibrational spectrum, which are applicable in various generalizations of the geometric quadrupole collective model [8,9], the self-consistent RMF model [13,26,27], and the quadrupole-octupole six-dimensional collective model of atomic nuclei with several local minima of the potential energy hypersurface, such that GTM calculations becomes rather cumbersome [12].

Note that the latter two-dimensional BVP has been solved using finite difference method (FDM) [30] and FEM [17] that was only part of the BVP in the

6D domain, where the potential energy and components of the metric tensor are given by 2×10^6 table values [12,31]. However, the FDM approach [30] did not obtain further generalization on the above multidimensional domain, while the elaborated FEM and PI-type Gaussian quadrature rules [32] have no restriction for further solving such BVP in the 6D domain. This obstacle has been one line of motivations in development and implementation of the above approach.

References

1. Bathe, K.J.: Finite Element Procedures in Engineering Analysis. Prentice-Hall Inc., Englewood Cliffs (1982)
2. Hess, P.O., Seiwert, M., Maruhn, J., Greiner, W.: General collective model and its application to 238_{92}U. Z. Phys. A Atoms Nuclei **296**, 147–163 (1980)
3. Libert, J., Quentin, P.: A general solution of the Bohr collective Hamiltonian. Z. Phys. A Atoms Nuclei **306**, 315–322 (1982)
4. Troltenier, D., Maruhn, J.A., Hess, P.O.: Numerical application of the geometric collective model. In: Langanke, K., Maruhn, J.A., Konin, S.E. (eds.) Computational Nuclear Physics 1, pp. 105–128. Springer, Heidelberg (1991). https://doi.org/10.1007/978-3-642-76356-4_6
5. Libert, J., Girod, M., Delaroche, J.-P.L.: Microscopic descriptions of superdeformed bands with the Gogny force: configuration mixing calculations in the A∼190 mass region. Phys. Rev. C **60**, 054301-1–054301-26 (1999)
6. Delaroche, J.-P., Girod, M., Gouttea, H., Libert, J.: Structure properties of even-even actinides at normal and super deformed shapes analysed using the Gogny force. Nucl. Phys. A **771**, 103–168 (2006)
7. Niksic, T., Li, Z.P., Vretenar, B.D., Prochniak, L., Meng, J., Ring, P.: Beyond the relativistic mean-field approximation. III. Collective Hamiltonian in five dimensions. Phys. Rev. C **79**, 034303-1–034303-19 (2009)
8. Ermamatov, M.J., Hess, P.O.: Microscopically derived potential energy surfaces from mostly structural considerations. Ann. Phys. **37**, 125–158 (2016)
9. Mardyban, E.V., Kolganova, E.A., Shneidman, T.M., Jolos, R.V.: Evolution of the phenomenologically determined collective potential along the chain of Zr isotopes. Phys. Rev. C **105**, 024321-1–024321-10 (2022)
10. Deveikis, A., et al.: Symbolic-numeric algorithm for calculations in geometric collective model of atomic nuclei. In: Boulier, F., England, M., Sadykov, T.M., Vorozhtsov, E.V. (eds.) CASC 2022. LNCS, vol. 13366, pp. 103–123. Springer, Cham (2022). https://doi.org/10.1007/978-3-031-14788-3_7
11. Muir, D.: Microscopic modelling of collective quadrupole excitations of nuclei. Ph.D. thesis, University of York, UK (2021). https://etheses.whiterose.ac.uk/29823/

12. Dobrowolski, A., Mazurek, K., Góźdź, A.: Rotational bands in the quadrupole-octupole collective model. Phys. Rev. C **97**, 024321-1–024321-11 (2018)

13. Deng, X.-Q., Zhou, S.-G.: Ground state and fission properties of even-a uranium isotopes from multidimensional-constrained relativistic mean field model. Int. J. Mod. Phys. **32**(10), 234004-1–234004-20 (2023)

14. Kumar, K., Baranger, M.: Complete numerical solution of Bohr's collective Hamiltonian. Nucl. Phys. A **92**, 608–652 (1967)

15. Troltenier, D., Maruhn, J.A., Greiner, W., Hess, P.O.: A general numerical solution of collective quadrupole surface motion applied to microscopically calculated potential energy surfaces. Z. Phys. A Hadrons Nuclei **343**, 25–34 (1992)

16. Troltenier, D.: Ph.D. thesis, J.W. Goethe-Universität, Frankfnrt/Main (1992). (Unpublished)

17. Gusev, A.A., et al.: Finite element method for solving the collective nuclear model with tetrahedral symmetry. Acta Phys. Pol. B Proc. Suppl. **12**, 589–594 (2019)

18. Gusev, A.A., et al.: Hermite interpolation polynomials on parallelepipeds and FEM applications. Math. Comput. Sci. **17**, 1–15 (2023). Article number: 18

19. Batgerel, B., et al.: Schemes of finite element method for solving multidimensional boundary value problems. J. Math. Sci. **279**, 738–755 (2024)

20. Vandandoo, U., Zhanlav, T., Chuluunbaatar, O., Gusev, A., Vinitsky, S., Chuluunbaatar, G.: High-Order Finite Difference and Finite-Element Methods for Solving Some Partial Differential Equations. Springer, Cham (2024)

21. https://www.wolfram.com/mathematica/

22. Gusev, A.A., et al.: Symbolic-numerical solution of boundary-value problems with self-adjoint second-order differential equation using the finite element method with interpolation hermite polynomials. In: Gerdt, V.P., Koepf, W., Seiler, W.M., Vorozhtsov, E.V. (eds.) CASC 2014. LNCS, vol. 8660, pp. 138–154. Springer, Cham (2014). https://doi.org/10.1007/978-3-319-10515-4_11

23. Gusev, A.A., Hai, L.L., Chuluunbaatar, O., Vinitsky, S.I., Derbov, V.L.: Solution of boundary-value problems using Kantorovich method. In: EPJ Web of Conferences, vol. 108, pp. 02026-1–02026-6 (2016)

24. Greiner, W., Maruhn, J.A.: Nuclear Models. Springer, Berlin (1995)

25. http://www.nndc.bnl.gov/ensdf/

26. Zhao, P.W., Li, Z.P., Yao, J.M., Meng, J.: New parametrization for the nuclear covariant energy density functional with a point-coupling interaction. Phys. Rev. C **82**, 054319-1–054319-14 (2010)

27. Nikšic, T., Paar, N., Vretenar, D., Ring, P.: DIRHB-a relativistic self-consistent mean-field framework for atomic nuclei. Comput. Phys. Commun. **185**, 1808–1821 (2014)

28. Tanaka, T., Nazmitdinov, R.G., Iwasawa, K.: Nonaxial octupole deformations in light $N = Z$ nuclei at high spins. Phys. Rev. C **63**, 034309-1–034309-111 (2001)

29. Nazmitdinov, R.G., Almehed, D., Dönau, F.: Dynamical moment of inertia and quadrupole vibrations in rotating nuclei. Phys. Rev. C **65**, 041307(R)-1–041307(R)-4 (2002)

30. Dobrowolski, A., Mazurek, K., Dudek, J.: Tetrahedral symmetry in nuclei: New predictions based on the collective model. Int. J. Mod. Phys. E **20**, 500–506 (2011)

31. Dobrowolski, A., Mazurek, K., Góźdź, A.: Consistent quadrupole-octupole collective model. Phys. Rev. C **94**, 0543220-1–0543220-20 (2016)

32. Chuluunbaatar, G., Chuluunbaatar, O., Gusev, A.A., Vinitsky, S.I.: PI-type fully symmetric quadrature rules on the 3-, ..., 6-simplexes. Comput. Math. Appl. **124**, 89–97 (2022)